Please do not adjust margins

COMMUNICATION

Electrocatalytic CO_2 reduction on earth abundant 2D Mo_2C and Ti_3C_2 MXenes

Received 00th January 20xx,
Accepted 00th January 20xx

DOI: 10.1039/x0xx00000x

Nuwan H. Attanayake,[a,b] Huta R. Banjade,[b,c] Akila C. Thenuwara,[a,b] Babak Anasori,[d,e] Qimin Yan,[b,c] Daniel R. Strongin. *[a,b]

Mo_2C and Ti_3C_2 MXenes were investigated as earth-abundant electrocatalyts for the the CO_2 reduction reaction (CO_2RR). Mo_2C and Ti_3C_2 exhibited Faradaic efficiencies of 90% (250 mV overpotential) and 65% (650 mV overpotential), respectively, for the reduction of CO_2 to CO in acetonitrile using an ionic liquid electrolyte. The use of ionic liquid 1-ethyl-2-methylimidazolium tetrafluoroborate as an electrolyte in organic solvent suppressed the competing hydrogen evolution reaction. Density functional theory (DFT) calculations suggested that the catalytic active sites are oxygen vacancy sites on both MXene surfaces. Also, a spontaneous dissociation of absorbed COOH species to a water molecule and absorbed CO on Mo_2C promote the CO_2RR.

The development of the electrochemical CO_2 reduction reaction (CO_2RR) would help to create a closed carbon cycle around the burning of fossil fuels and potentially mitigate environmental problems resulting from the release of CO_2 to the atmosphere.[1, 2] The utility of an efficient CO_2RR would not only include the suppression of greenhouse gas emission, but it could potentially extend to the generation of industrially valuable chemicals that are now obtained through the petroleum industry.[3, 4] Development of earth-abundant and relatively inexpensive catalysts, however, that efficiently drive the electrochemical CO_2RR to produce fuels and commodity chemicals still remains a challenge.

Over the past few decades, the electrochemical CO_2RR to convert CO_2 to CO has been evaluated on many heterogeneous catalysts, although only a few materials have shown promise as potential catalysts that can be scaled up to be part of an efficient industrial process. Precious metals, such as silver and gold, have been shown to be able to electrochemically reduce CO_2 to CO at relatively low overpotential values with high faradaic efficiency (FE). These metals, however, are not earth-abundant and could be prohibitively expensive if used at a commercial scale.[5-8]

In the current study we investigated the ability of Mo_2CT_x and $Ti_3C_2T_x$ (MXenes), comprised of earth abundant elements, to catalyze the electrochemical CO_2RR. MXenes are a class of 2D materials comprised of transition metal carbides, nitrides, and carbonitrides derived from ternary carbides and nitrides, mostly MAX phases.[9-12] The name MAX is derived from the composition of the material where "M" denotes an early transition metal, "A" an A-group metal such as aluminium or gallium and "X" denotes carbon and/or nitrogen. MXenes have the general formula $M_{n+1}X_nT_x$ (n=1-4) where T_x represents the surface functional groups, mostly –OH, –F, and =O.[11, 13, 14] The T_x notation, however, is dropped hereafter from the general formula for brevity. Relevant to the current study, a prior density functional theory (DFT) computational study suggested that M_3C_2 MXenes are promising materials for the CO_2RR.[15] The experimental studies discussed in this contribution evaluate the Mo_2C and Ti_3C_2 MXenes for the CO_2RR.

Mo_2C and Ti_3C_2 used in this study were produced from their respective ternary carbide precursors using preparation methods outlined in prior studies (see SI).[9, 13, 16] In brief, Mo_2C was formed by etching the Ga layers from the layered ternary carbide, Mo_2Ga_2C, in a solution containing LiF/HCl to form a colloidal suspension of delaminated Mo_2C (denoted as d-Mo_2C). Ti_3C_2 was obtained by exfoliating the corresponding Ti_3AlC_2 MAX phase with LiF/HCl to form a delaminated Ti_3C_2 (denoted as d--Ti_3C_2). Microscopy results shown in prior contributions that developed these synthetic protocols show the samples to have a layered structure.[10, 14, 16-18]

Experiments were conducted to determine the electrocatalytic activity of the MXenes for the CO_2RR with a standard 3-electrode cell setup using MXene coated glassy carbon electrodes (see SI for preparation details). Figure 1 exhibits a polarization plot obtained by linear sweep voltammetry (LSV) for d-Mo_2C in CO_2 saturated acetonitrile

[a.] Department of Chemistry, Temple University, 1901 N. 13th Street, Philadelphia, PA 19122 (USA)
[b.] Center for Complex Materials From First Principles (CCM)
[c.] Department of Physics, Temple University, 1925 N 12th St, Philadelphia, PA 19122 (USA)
[d.] Department of Materials Science and Engineering, and A.J. Drexel Nanomaterials Institute, Drexel University, Philadelphia, PA 19104 (USA)
[e.] Integrated Nanosystems Development Institute, and Department of Mechanical and Energy Engineering, Purdue School of Engineering and Technology, Indiana University–Purdue University Indianapolis, Indianapolis, IN 46202 (USA).

†Electronic Supplementary Information (ESI) available: [details of any supplementary information available should be included here]. See DOI: 10.1039/x0xx00000x

This is the author's accepted manuscript of the article published in final edited form as:

Attanayake NH, Banjade HR, Thenuwara AC, Anasori B, Yan Q, Strongin DR. Electrocatalytic CO2 reduction on earth abundant 2D Mo2C and Ti3C2 MXenes. ChemComm. 2020;57(13). doi:10.1039/d0cc05822j

Please do not adjust margins

(MeCN) containing the ionic liquid (IL), 1-Ethyl-3-methylimidazolium tetrafluoroborate ([EMIM]BF_4. Also included is a polarization curve for a clean glassy carbon electrode in the CO_2 saturated MeCN/IL solution and data for *d*-Mo_2C in a CO_2-free (nitrogen-sparged) MeCN/IL environment. The *d*-Mo_2C coated electrode in a CO_2-free (N_2 saturated) MeCN/IL solution does show an onset potential for current flow at about -2.1 V. Analysis of the reaction vessel headspace with gas chromatography (GC, see SI for experimental details) shows

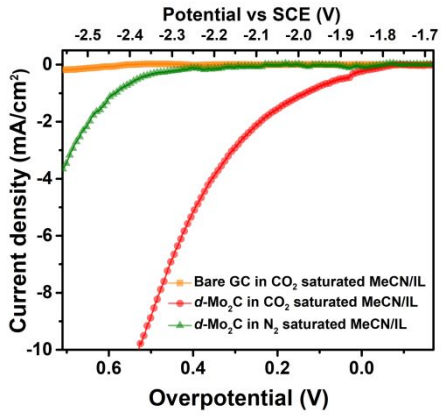

Figure 1: Comparison of the polarization plots of *d*-Mo_2C in MeCN/IL saturated with CO_2 or N_2. SCE denotes saturated calomel electrode and GC denotes glassy carbon.

hydrogen product in this non-aqueous reaction environment (SI, Figure S1). While the MeCN was dried before use, the presence of some residual water cannot be ruled out as the proton source. Importantly, however, is that the polarization data for *d*-Mo_2C exhibits a lower onset potential (-1.85 V vs SCE) and higher cathodic current with increasing potential compared to *d*-Mo_2C (-2.2 V onset) in the CO_2-free environment. We therefore attribute the lower onset potential and higher cathodic currents to CO_2RR chemistry. Support for this contention comes from a GC analysis of the reaction cell headspace, which shows primarily CO product (SI, Figure S1) in the CO_2 saturated environment.

Data presented in Figure 2 allows a comparison of the polarization curve for *d*-Mo_2C to the *d*-Ti_3C_2 MXene and nano-dimensioned silver (<100 nm). While the *d*-Mo_2C electrocatalyst exhibits an onset potential as low as –1.85 V vs SCE (~0 mV overpotential), the onset for the *d*-Ti_3C_2 MXene occurs at a higher potential of -2.2 V vs SCE. It is noted that *d*-Ti_3C_2 MXene requires a potential of ~-2.5 V (overpotential ~650 mV) before CO product is detected as a reaction product. Based on this comparison the *d*-Mo_2C is a better CO_2RR electrocatalyst than *d*-Ti_3C_2. The electrocatalytic activity of *d*-Mo_2C is similar to that of the precious metal silver under our experimental conditions. In particular, the polarization data associated with a silver nanoparticle electrode exhibits an onset ~-1.85 V (vs SCE) for the CO_2RR, similar to *d*-Mo_2C. Furthermore, the similarity of the Tafel slope values for *d*-Mo_2C and Ag (SI, Figure S2) suggests that the mechanism for the electrochemical reduction of CO_2 is similar on both surfaces. Chronoamperometric measurements (constant voltage) for *d*-Mo_2C, *d*-Ti_3C_2, and silver were carried out in a two-compartment cell to determine the stability of the electrocatalysts and their FE for CO production. The anode and

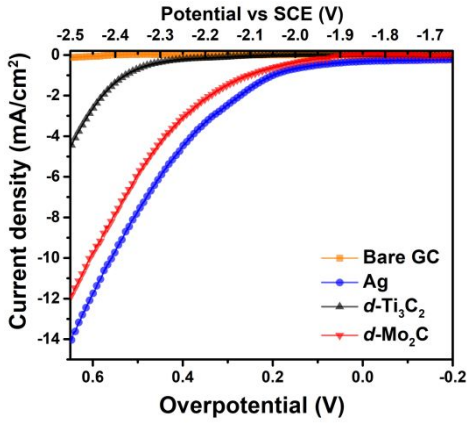

Figure 2: Polarization plot of the *d*-Mo_2C, *d*-Ti_3C_2 MXenes and Ag nanoparticles in CO_2 saturated MeCN/IL

the cathode compartments were separated by an anion exchange Nafion membrane. This membrane kept any reduction products in the cathode side from diffusing to the anode compartment. GC analysis of the headspace gas showed that CO was the primary gaseous product formed from the CO_2-RR (small amount of H_2 was also present). Analysis of the headspace during the electrochemistry of *d*-Mo_2C in MeCN/IL without CO_2 present showed no CO product ruling out the possibility of CO resulting from the decomposition of the MeCN/IL. An analysis of the electrolyte with 1H-NMR after the CO_2RR for the CO_2/Mo_2C system showed no evidence for solution phase reaction products or decomposition of the MeCN/IL (SI, Figure S3).

The stability of the *d*-Mo_2C electrocatalyst for CO_2RR was investigated by determining the cathodic current as a function of potential (voltages used: -2.14, -2.24, -2.34, -2.44, -2.54 and -2.64 V vs SCE) for 0.5 h. The stability of the *d*-Mo_2C MXene catalyst was excellent at the cathode potentials between -2.0 and -2.3 V based on the constant cathodic current in this range of voltages (Figure 3a). An increase in the current density was observed at greater voltages (-2.5 and -2.6 V, Figure 3a), which corresponds with the increase in the HER. For the Ti_3C_2 MXene, we observe a reduction in the activity of the catalyst for HER at applied potentials higher than -2.6 V. XPS after reaction at this relatively high potential shows that there is a reduction of surface Ti-O (see XPS results in SI, figure S6 and S7). DFT calculations presented below suggest that such an oxygen deficient *d*-Ti_3C_2 surface (at the higher potential) may over bind reaction species decreasing HER activity. Figure 3b exhibits the FE of *d*-Mo_2C, *d*-Ti_3C_2, and Ag nanoparticles for CO production during the CO_2RR as a function of cathodic voltage. Up until a voltage of -2.24 V *d*-Mo_2C exhibited a FE of ~90% for CO production, similar to the Ag nanoparticle catalyst. At higher overpotentials the FE associated with *d*-Mo_2C drops (~80% at 600 mV and 50% at 750 mV), while the Ag catalyst efficiency remains at 90%. The decrease in faradaic efficiency for CO production is mirrored by a corresponding increase in H_2 product evolution at these higher overpotentials. The

This journal is © The Royal Society of Chemistry 20xx

overpotential for initial CO production during CO_2RR for *d*-Ti_3C_2 was ~-650 mV, significantly higher than the -200 mV overpotential that resulted in CO production on *d*-Mo_2C. The activity of the *d*-Ti_3C_2 for CO production is maintained at the potentials studied for times approaching 0.5 h (SI, Figure S4). Prior research has shown that in an acidic aqueous solution the hydrogen evolution reaction (HER) occurs with a lower

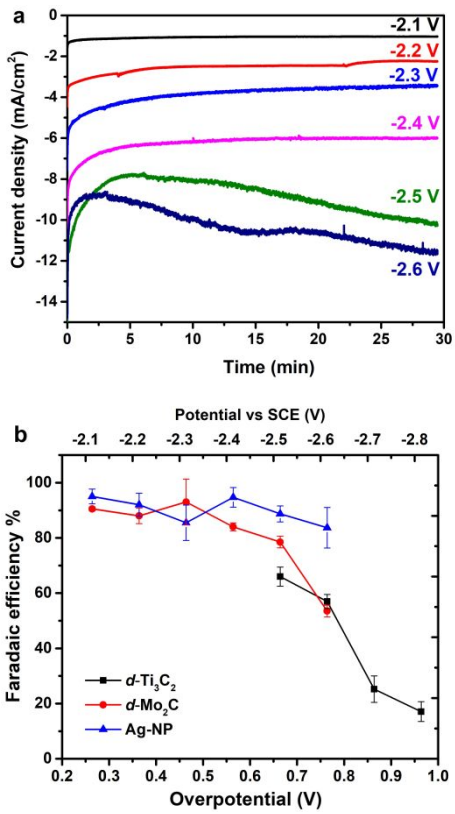

Figure 3: a) Chronoamperometric curves for d-Mo_2C MXene (potentials cited are vs SCE) and b) FE vs overpotential plots for *d*-Mo_2C, *d*-Ti_3C_2 MXenes and Ag nano particles (Ag-NP).

overpotential on *d*-Mo_2C than on *d*-Ti_3C_2.[14] In the present study the HER was suppressed by using the aprotic solvent.[19-22] Experiments that investigated the electrocatalytic activity of *d*-Mo_2C and *d*-Ti_3C_2 in CO_2 saturated aqueous IL resulted in only H_2 production (SI, Figure S5) suggesting that the CO_2RR is not viable in the aqueous environment. These results taken together suggest that the active sites on the MXenes that catalyze the reduction of CO_2 to CO are likely the same sites that drive the HER under aqueous conditions.[14] ECSA estimations (SI, Figure 8) based on the double layer capacitance show that the active area for both Mo_2C and Ti_3C_2 are comparable, thus the difference in the activity is attributed to the difference in their intrinsic activities.

Density functional theory (DFT) based computations were carried out in order to shed light on the mechanism for the CO_2RR on Mo_2C and Ti_3C_2. We investigated the energetics of elementary reaction steps for the CO_2RR on model pristine and oxygen terminated MXene surfaces. For bare (no surface oxygen) Mo_2C and Ti_3C_2 surfaces, binding energy calculations show that CO_2, CO and other reaction intermediates such as *COOH have a very strong chemisorption which is consistent with previous studies.[15, 23] The reaction free energy diagram for the electrochemical reduction of CO_2 on these bare surfaces is presented in Figure S7 (SI). Inspection of the free energy diagram suggests that there is an over-binding of the CO_2 reduction intermediates, CO and COOH, on bare Ti_3C_2 and Mo_2C. Therefore, it is not expected that a significant amount of CO gas can be generated from the bare surfaces of Ti_3C_2 and Mo_2C. X-ray photoelectron spectroscopy (XPS), however, suggests that the MXene surfaces used in our study are largely oxygen terminated consistent with previous studies of Mo_2C that suggest that such a termination stabilizes the bare surface (SI, Figure S9).[14] Furthermore, it is predicted that the oxygen functionalized Mo_2C is more stable than those terminated by other functional groups.[24] A similar conclusion has been arrived at for oxygenated surfaces of Ti_3C_2.[25] Our results indicate that a fully O-terminated surface does not capture CO and CO_2 (SI, Figure S10), which indicates a too weak binding for the CO_2RR. Thus, we looked at other plausible sites for the CO_2RR on these MXenes.

We chose to carry out DFT calculations on the model MXene oxygen terminated surface with oxygen vacancies to study the mechanism of electrochemical reduction of CO_2 to CO. Such sites are plausible reaction sites for the CO_2RR. They can be generated during the exfoliation and delamination of

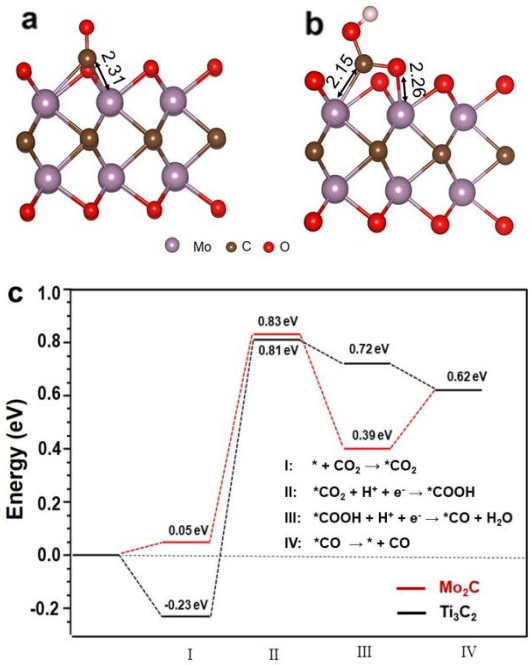

Figure 4: (a) CO absorbed at the oxygen vacancy on Mo_2C. (b) COOH absorbed at the oxygen vacancy on Mo_2C (red-oxygen atoms, brown-carbon atoms, white-hydrogen and purple- molybdenum atoms). The distances between molecules and surfaces are noted in the plots (in Angstrom). (c) The free energy diagram for CO_2 reduction reaction at the oxygen vacancy on Ti_3C_2 (in black) and Mo_2C (in red) calculated using the PBE functional.

MXenes and under electrochemical reduction conditions.[16] Figure 4a and 4b exhibits the relaxed structural configurations used to model the Mo_2C surface with an oxygen vacancy and CO (Figure 4a) and COOH (Figure 4b) adsorbed at the vacancy site. Our study indicates that CO_2 reduction can be realized by a standard three-step process which includes the activation of CO_2 to form *COOH (* denotes adsorbed) through the first electron/proton transfer and the dissociation of COOH to *CO and H_2O as products resulting from the second transfer. The final step is accompanied by the detachment of CO from the surface. The computed free energy diagram for oxygen terminated Ti_3C_2 and Mo_2C surfaces with an oxygen vacancy are shown in Figure 4c. CO_2 exhibits weak binding at the vacancy on oxygen terminated Ti_3C_2, while it is physically adsorbed at the oxygen vacancy on the oxygen terminated Mo_2C. The activation of $^*CO_2$ to $^*COOH$ in the first hydrogenation step demands a free energy input of 1.04 and 0.78 eV for the case of Ti_3C_2 and Mo_2C, respectively. The calculated free energy diagram suggests that, in the second protonation process, the $^*COOH$ intermediate absorbed on both surfaces will spontaneously dissociate and form H_2O and *CO. During the electrochemical reduction of CO_2 to CO, the rate limiting step is the first electron/proton transfer step, i.e., the activation of CO_2 to form *COOH. The rate limiting step demands 0.26 eV less free energy input for Mo_2C than in Ti_3C_2. To evaluate the effects of van der Waals interactions on the energetics, we applied the dispersion corrections of Grimme's DFT-D3 and found that the main conclusion in the manuscript still holds true (see the SI for details).[26] Therefore, we conclude that Mo_2C is a more promising catalyst that requires a lower overpotential for the electrochemical reduction of CO_2 to CO, which is in line with our experimental observations.

Conflicts of interest

There are no conflicts to declare.

Acknowledgements

The authors acknowledge Prof. Yury Gogotsi (Department of Materials Science and Engineering, and A.J. Drexel Nanomaterials Institute, Drexel University, Philadelphia, PA 19104 (USA)) for his valuable insight and providing MXene samples for the research.

Funding Sources

This work was supported by the Center for the Computational Design of Functional Layered Materials, an Energy Frontier Research Center funded by the U.S. Department of Energy, Office of Science, Basic Energy Sciences under Award # DE-SC0012575.

Notes and references

1. N. S. Lewis and D. G. Nocera, *Proc. Nat. Acad. Sci.*, 2006, **103**, 15729-15735.
2. J. O. M. Bockris, *Int. J. Hydrog. Energy*, 2013, **38**, 2579-2588.
3. K. P. Kuhl, T. Hatsukade, E. R. Cave, D. N. Abram, J. Kibsgaard and T. F. Jaramillo, *J. Am. Chem. Soc.*, 2014, **136**, 14107-14113.
4. P. N. R. Vennestrøm, C. M. Osmundsen, C. H. Christensen and T. Esben, *Angew. Chem. Int. Ed.*, 2011, **50**, 10502-10509.
5. Y. Hori, H. Wakebe, T. Tsukamoto and O. Koga, *Electrochimica Acta*, 1994, **39**, 1833-1839.
6. H.-R. M. Jhong, S. Ma and P. J. A. Kenis, *Current Opinion in Chemical Engineering*, 2013, **2**, 191-199.
7. A. Salehi-Khojin, H.-R. M. Jhong, B. A. Rosen, W. Zhu, S. Ma, P. J. A. Kenis and R. I. Masel, *J. Phys. Chem. C* 2013, **117**, 1627-1632.
8. C. E. Tornow, M. R. Thorson, S. Ma, A. A. Gewirth and P. J. A. Kenis, *J. Am. Chem. Soc.*, 2012, **134**, 19520-19523.
9. M. Naguib, O. Mashtalir, J. Carle, V. Presser, J. Lu, L. Hultman, Y. Gogotsi and M. W. Barsoum, *ACS Nano*, 2012, **6**, 1322-1331.
10. M. Alhabeb, K. Maleski, B. Anasori, P. Lelyukh, L. Clark, S. Sin and Y. Gogotsi, *Chem. Mater.*, 2017, **29**, 7633-7644.
11. B. Anasori, M. R. Lukatskaya and Y. Gogotsi, *Nat Rev Mater.*, 2017, **2**, 16098.
12. M. Naguib, V. N. Mochalin, M. W. Barsoum and Y. Gogotsi, *Adv. Mater.*, 2014, **26**, 992-1005.
13. F. M. Romer, U. Wiedwald, T. Strusch, J. Halim, E. Mayerberger, M. W. Barsoum and M. Farle, *RSC Adv.*, 2017, **7**, 13097-13103.
14. Z. W. Seh, K. D. Fredrickson, B. Anasori, J. Kibsgaard, A. L. Strickler, M. R. Lukatskaya, Y. Gogotsi, T. F. Jaramillo and A. Vojvodic, *ACS Energy Lett.*, 2016, **1**, 589-594.
15. N. Li, X. Chen, W.-J. Ong, D. R. MacFarlane, X. Zhao, A. K. Cheetham and C. Sun, *ACS Nano*, 2017, **11**, 10825-10833.
16. J. Halim, S. Kota, M. R. Lukatskaya, M. Naguib, M.-Q. Zhao, E. J. Moon, J. Pitock, J. Nanda, S. J. May, Y. Gogotsi and M. W. Barsoum, *Adv. Funct. Mater.*, 2016, **26**, 3118-3127.
17. A. Lipatov, M. Alhabeb, M. R. Lukatskaya, A. Boson, Y. Gogotsi and A. Sinitskii, *Advanced Electronic Materials*, 2016, **2**.
18. X. Sang, Y. Xie, M.-W. Lin, M. Alhabeb, K. L. Van Aken, Y. Gogotsi, P. R. C. Kent, K. Xiao and R. R. Unocic, *ACS Nano*, 2016, **10**, 9193-9200.
19. B. A. Rosen, A. Salehi-Khojin, M. R. Thorson, W. Zhu, D. T. Whipple, P. J. A. Kenis and R. I. Masel, *Science*, 2011, **334**, 643-644.
20. M. Asadi, B. Kumar, A. Behranginia, B. A. Rosen, A. Baskin, N. Repnin, D. Pisasale, P. Phillips, W. Zhu, R. Haasch, R. F. Klie, P. Král, J. Abiade and A. Salehi-Khojin, *Nat. Comm.*, 2014, **5**, 4470.
21. J. Medina-Ramos, J. L. DiMeglio and J. Rosenthal, *J. Am. Chem. Soc.*, 2014, **136**, 8361-8367.
22. J. T. Feaster, A. L. Jongerius, X. Liu, M. Urushihara, S. A. Nitopi, C. Hahn, K. Chan, J. K. Nørskov and T. F. Jaramillo, *Langmuir*, 2017, **33**, 9464-9471.
23. A. D. Handoko, K. H. Khoo, T. L. Tan, H. Jin and Z. W. Seh, *J. Mater. Chem. A*, 2018, **6**, 21885-21890.
24. M. Ashton, K. Mathew, R. G. Hennig and S. B. Sinnott, *J. Phys. Chem. C*, 2016, **120**, 3550-3556.
25. C. Shi, H. A. Hansen, A. C. Lausche and J. K. Nørskov, *Phys. Chem. Chem. Phys.*, 2014, **16**, 4720-4727.
26. S. Grimme, J. Antony, S. Ehrlich and H. Krieg, *The Journal of Chemical Physics*, 2010, **132**, 154104.

This journal is © The Royal Society of Chemistry 20xx

TOC graphic

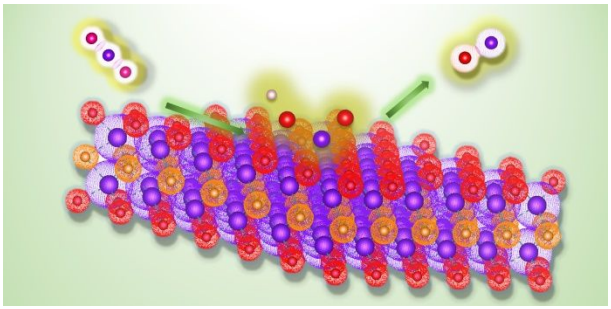

TOC abstract:

The electrocatalytic reduction of CO_2 to CO on the Mo_2C and Ti_3C_2 MXenes. DFT calculations show that surface oxygen vacancies are reaction active sites.